LAWRENCE
LIVERMORE
NATIONAL
LABORATORY

UCRL-JRNL-235640

Imperfect Crystal and Unusual Semi-Conductor: Boron, a Frustrated Element

T. Ogitsu, F. Gygi, J. Reed, E. Schwegler, G. Galli

October 18, 2007

Journal of the American Chemical Society

Disclaimer

Imperfect crystal and unusual semi-conductor: Boron, a frustrated element

Tadashi Ogitsu[1], François Gygi[1,2], John Reed[1], Eric Schwegler[1], and Giulia Galli[1,2]

[1]*Lawrence Livermore National Laboratory, CA, USA;*

[2]*University of California, Davis, CA, USA.*

All elements, except for helium, appear to solidify into crystalline forms at zero temperature, and it is generally assumed that the introduction of lattice defects results in a loss of internal energy. Here we suggest that boron is another exception. By using lattice Monte Carlo techniques combined with *ab-initio* calculations, we find that the most stable phase of boron (β-boron), is non-crystalline, with a unique combination of partially occupied sites. The inclusion of defects stabilizes β-boron by converting two-center bonds into the three-center bonds characteristic of many boron compounds, and by adjusting its Fermi level to the top of the valence band. These defects are also responsible for the presence of localized, non-conductive electronic states in the optical gap.

In the periodic table boron occupies a peculiar, crossover position: on the first row, it is surrounded by metal forming elements on the left and by non-metals on the right. In addition, it is the only non-metal of the third column. Therefore, it is perhaps not surprising that the crystallographic structure and topology of its thermodynamically stable allotrope (β-boron, space group $R\bar{3}m$)[1,2,3] is not shared by any other element, and is extremely complex. It is experimentally known that β-boron contains many partially occupied sites (POS), with occupation rates that are not integer numbers, varying roughly from 2% to 75% from site to site[3]. The most accurate experimental estimate of the number of atoms in the hexagonal cell is 320.1[3], which corresponds to approximately 106 2/3 atoms per rhombohedral cell, implying a violation of rhombohedral symmetry. No experimental evidence of lower symmetry and/or longer-range ordering, presumably detectable by X-ray diffraction, has been reported. Therefore, it is reasonable to assume that at finite temperature the presence of POS break the translational symmetry of β-boron. It remains an open question whether this imperfect crystal is also the most stable structure of elemental boron at zero *T*; if so, boron is the first known example of an element not crystallizing in a fully ordered form.

A simpler allotrope of boron is the α-phase, that has a crystalline structure with 12 atoms per rhombohedral cell (space group $R\bar{3}m$ and no POS). To date, there are no experimental data discriminating between the relative stability of the boron allotropes[4,5]. Large kinetic barriers and/or high melting temperatures (T_{melt} = 2349 K for β-boron) have possibly prevented accurate measurements by unambiguous techniques, such as calorimetry. α-rhombohedral boron has been extensively examined by *ab-initio* density

functional theory (DFT) calculations, and there are also a number of *ab-initio* investigations where α- and β-boron total energies[6,7] have been directly compared[8,9,10,11]. In the vast majority of these studies a small subset of the possible POS configurations were accounted for and it was concluded that α-boron is more stable than β-boron at zero temperature[8,9,11]. However, one recent investigation indicates that it is possible to find an arrangement of POS in β-boron, that makes it more stable than the α-phase[10]. Due to the astronomical number of possible combinations of POS configurations, in all of the theoretical investigations that have appeared so far, the choice and occupation of POS have been based on semi-empirical electron counting rules, experimentally measured occupation rates, and *ab-initio* studies on small gas-phase boron clusters. The lack of a systematic, non-empirical optimization has so far prevented a microscopic description of the mechanisms by which defects (*i.e.* POS) may stabilize β-boron and ultimately an understanding of why such an unusual ground state should be energetically favored.

In this paper, we used a combination of lattice model Monte Carlo techniques and *ab-initio* Density Functional Theory (DFT) total energy calculations to carry out the first global configuration space search of POS occupations in β-boron. The results of this optimization procedure allowed us to identify a series of β-boron structures degenerate in energy and more stable than α-boron at zero *T*. These are disordered structures with intrinsic doping, exhibiting localized electronic levels within the optical gap. The presence of POS enables the conversion of conventional two-center bonds, present in non-defective β-boron, into three-center bonds characteristic of many boron compounds[12,13].

Fig.1 illustrates the building blocks of β-boron. The main backbone can be viewed as 20 B_{12} icosohedra located at the corners and edges of a rhombohedral cell with two B_{28} clusters connected by an interstitial atom in the center. Within this backbone there are 15 inequivalent sites (*i.e.* not related by symmetry operations), which we refer to as B1-B15, following previous works[2,3]. The B13 site, which is located in the B_{28} clusters next to the interstitial atom (see Fig 1b), is a vacancy-type POS, known from experiment to have an occupation of approximately 75%[2,3]. If all of the B13 sites were fully occupied, β-boron would be a perfect crystal with 105 atoms in a rhombohedral unit cell (commonly referred as hR105). In addition to the main backbone, five additional inequivalent sites B16-B20 (see Fig. 1c-g) have been identified as POS by experiment[14]. In all of the previous *ab-initio* studies where β-boron was found to be higher in energy than α-boron, the atomic density was an approximation of the experimental value, corresponding to 320 atoms per hexagonal cell, due to computational limitations (and the B17-B20 POS were not taken into account[15]); on the other hand, in the one *ab-initio* study where β-boron was found to be more stable than α-boron, the experimental atomic density was used and some of the B17-B20 POS were examined[16].

In order to carry out an optimization of the β-boron structure including all of the POS (B13, B16-B20), a cost-efficient global configuration space search scheme is needed due to the huge number of possible POS configurations. There are $\begin{bmatrix} 504 \\ 92 \end{bmatrix}$ possible POS configurations[17] for the 1280 atom supercell that we have used in this work. Therefore, we employed an optimization procedure that couples *ab-initio* DFT and Cluster Expansion / Monte Carlo (CEMC) techniques[18,19,20] (a more detailed description can be found in the Supplemental Material 3). This computational procedure is similar to the

approach often used to determine the composition and location of impurities or defects in a known crystal lattice[20] or the composition and ordering of species in an alloy[18,19]. In our case, we mapped the POS occupation numbers onto a spin Hamiltonian and expressed the total energy of the β-phase as a linear combination of correlations in occupancy between different sets of POS. The coefficients of such an expansion were fitted to *ab-initio* total energy data obtained for a large set of configurations. Our optimization strategy consists of the following steps: (i) We considered rhombohedral cells with both 106 and 107 atoms (hR106 and hR107, respectively, corresponding to 318 and 321 atom/hexagonal cells, thus bracketing the number of atoms/cell proposed experimentally, i.e. ~ 320). The total number of possible configurations (~150 million in the case of hR107) was restricted to symmetrically independent and physically relevant ones (see Supplemental Material), thus reducing their number to 2591. (ii) Using the correlation coefficients obtained by fitting these 2591 total energies, we constructed a spin Hamiltonian for supercells containing 1280 atoms (referred to as hR1280 hereafter). (iii) Monte Carlo simulated annealing cycles with the Metropolis algorithm were then performed for this Hamiltonian. (iv) The most stable hR1280 structures obtained by the MC annealing procedure were further optimized using *ab-initio* methods, by relaxing both atomic positions and cell parameters[21]. (v) The new *ab-initio* results were inserted back into the database fit to improve the model, and further iterations of steps (iii) and (iv) were carried out[22].

By using this coupled CEMC/*ab-initio* procedure we identified a family of optimized structures (see Fig. 2) with very similar total energies that are several meV/atom lower than that of α-boron (the total energy of the most stable one is 7.5

meV/atom below that of α-boron). These total energies were computed by including the zero point energy (ZPE) contribution evaluated from *ab-initio* full phonon dispersion calculations[23]. The total energies of these stable structures are within a few meV/atom of each other, suggesting a highly degenerate character of the β-boron ground state.

The key features found in the stable hR1280 structures are that specific sets of POS are always occupied, and that the POS occupation configurations exhibit clear short-range correlations that are responsible for structural stabilization. In particular, B17 and B18 POS are always present in the lowest energy structures, and the absence of B19 and/or B20 POS only lead to a negligibly small increase in the total energy of the β-phase (see Table S3.1 of the Supplemental Material). The B17 and B18 POS in hR1280 always appear in a paired configuration next to two B13 vacancies, similar to previous predictions by Slack *et al.*[3]. However, in our stable structures the location of the B13 vacancies are quite different from those suggested in Ref. [3]; we find the inclusion of two B13 vacancies on the same B_{28} cluster to be highly unfavorable, as compared to distributing them on opposite sides of the interstitial atom linking two B_{28} clusters (see Fig. 1b). We note that the occupation of B19 or B20 POS only takes place when there is a single B13 vacancy nearby.

In order to rationalize the observed trends in the POS occupations, we analyzed the bonding properties of β–boron by means of maximally localized Wannier functions (MLWF)[24], which are analogous to the Boys orbitals commonly used in quantum chemistry to investigate bonding properties of compounds. (See Supplemental Material 5 for the calculation procedure used here, as well as a discussion on the relation between MLWFs and bonding properties.) Fig. 3a shows the MLWFs for the perfect β-boron

structure (with no POS), which are located either on bonds within icosahedra (intra-B_{12} and intra-B_{28} bonds) or on inter-icosahedral bonds (B_{12}-B_{12} linkages, and B_{12}-B_{28} linkages). The occupation of these orbitals can be defined by using the unitary transformation relating MLWFs and electronic eigenstates. With this procedure, we find that the inter-icosahedral bonds are more electron deficient than intra-icosahedral bonds, particularly the ones corresponding to the B_{12}-B_{12} linkages[25], which surrounds the B16 POS sites. From Fig. 3b-c it is clear that the inclusion of B13 vacancies and B16 POS in a perfect β-lattice leads to dramatic changes in the distribution of electron deficient bonds within the lattice. In both of the configurations shown, the originally electron deficient two-center bonds in the B_{12} linkages are converted to fully occupied three-center bonds due to the presence of B16 POS. In addition, the presence of a B13 vacancy causes the electron deficiency character of bonds to be shifted to the B_{28} units.

If one assumes that the most electron deficient bonds are likely to be the most chemically active, then it is reasonable to expect that the POS nearby the electron deficient bonds will be preferentially occupied. This is precisely consistent with what we observe in the optimized, stable hR1280 configurations: When one B13 vacancy is present in a $(2B_{28})$B unit, the closest B19 POS is occupied. In this case, the formation of three-center bonds around the B19 atom is clearly observed (Fig 3d), and simultaneously, all the electron deficient bonds in the B_{28} unit are now fully saturated (compare Fig 3b and 3d). Essentially the same trends in the electronic structure are found when the B20 site is occupied next to a B13 vacancy (see Supplemental Material 5). When two B13 vacancies are present in a $(2B_{28})$B cluster, the nearby B17-B18 paired sites are occupied,

and the saturation of electron deficient bonds occurs (compare Fig 3c and 3e). However, the formation of unambiguous three-center bonding is not as clear.

Jemmis *et al*. pointed out two important facts about bonding in solid boron, derived from empirical *mno* rules, and confirmed by *ab-initio* total energy calculations on the isolated B_{12} and $(2B_{28})B$ clusters[25]. They found that B_{12} clusters are more electron deficient than B_{28} (this can also be seen in Fig. 4a) and that the full occupation of B13 is energetically unfavorable in B_{28} clusters, which we confirmed with our solid phase calculations. The relatively high occupation rate of B16 is clearly related to the electron deficiency imbalance between B_{12} and B_{28}, while the smaller B17-B20 occupations are controlled by the number of available B13 vacancies.

To summarize, we have identified two distinct stabilization mechanisms: one involves the conversion of two-center to three-center bonding near B16, B19, and B20 sites, and the other leads to B17-B18 pairing next to B13 vacancies. Interestingly, the former mechanism amounts to perfect self doping, as each POS atom brings three valence electrons without changing the number of valence states (three, two-center bonds are converted into three, three-center bonds); the latter mechanism corresponds instead to a partial self doping effect because an additional bonding state is introduced into the valence band (see the Supplemental Material 5 and 7 for additional details). Self-doping in β-boron is an interesting consequence of the POS occupation, also leading to the adjustment of the Fermi level to the excitation gap[26]. Recently, Tang and Ismail-Beigi studied the stable forms of boron in 0-D (clusters) and 2-D (sheets) using DFT total energy calculations, and found that the balance between three- and two-center bonds leads to a full occupation of in-plane bonding states (with no occupied anti-bonding

orbitals)[27]. This is essentially the same mechanism that we have found to occur in the presence of POS sites in the 3-D β-boron structure, with the exception of the B_{28} unit, which has an intrinsic instability at the B13 site[25].

Finally, we compare our findings on the electronic structure of β-boron with experimental observations. The comparison is qualitative, since experimentally, β-boron is usually prepared from the melt, and therefore actual β-boron samples at low-*T* are likely to contain meta-stable POS configurations that are frozen into their high-*T* equilibrium states. Our *ab-initio* molecular dynamics simulations suggest that the onset of diffusion of the POS atoms occurs at roughly 1000 K. The electronic structures of the hR1280 systems considered in our calculations vary significantly, in particular near the Fermi level, even for geometries with similar energies. However, there are some general trends that can be identified. The most stable structures tend to have the largest gap with the fewest number of intrinsic gap levels, while the meta-stable structures tend to have a large number of gap levels (see Supplemental Material 7). Most of the experimental reports indicate the presence of gap levels[28,29], consistent with our results. Our most stable hR1280 structure has an electronic band gap of 0.8 eV, which is smaller than experiment (1.5 to 1.6 eV)[28,29]. However, considering the possible uncertainty in the structure of real β-boron samples at finite *T*, and the well-known tendency of the local density approximation to underestimate gaps, this level of agreement is reasonable. We have also computed the optical conductivity of one of the hR1280 structures within the Kubo-Greenwood formalism[30,31]. Our estimate for the DC conductivity is $50 \pm 50 [1/\Omega\text{cm}]$ at T=300 K, while the experimental value within the impurity free limit is of the order of $10^{-8} [1/\Omega\text{cm}]$[3]. As the Kubo-Greenwood formula does not account for

inelastic electron-phonon scattering, our estimate should be considered as an upper bound value, and as such the agreement with experiment is satisfactory. As indicated in Fig. 4, our computed low conductivity in the presence of gap states is due to the highly localized nature of these states, which resemble those found in a disordered semiconductor.

It is interesting to note that the persistence of B17-B18 pairs in our most stable hR1280 configurations always results in the introduction of additional bonding states. In contrast, the occupation of B19 and/or B20 POS does not modify the number of valance states (see Supplemental Material 5). This implies that if the ground state atomic density is exactly 320 atoms per hexagonal cell, and the true ground state structure indeed possesses B17-B18 pairs, then the ground state of elemental boron cannot be a perfect semiconductor.

Although boron is the only element whose stable solid structure is composed of icosahedral building blocks, we note that other 3rd group elements exhibit a well-known tendency to form icosahedral quasicrystal compounds, such as aluminum-magnesium-zinc[32] or gallium-magnesium-zinc[33]. It is generally believed that the Hume-Rothery mechanism plays an important role in the stabilization of these systems[34,35,36,37], where the presence of mid-range ordering leads to an opening of a pseudo gap in the free electron like density of states of an aperiodic intermetallic compound; this in turn causes a preference for stoichiometries where the Fermi level coincides with the minimum of the pseudo gap[35]. An analogy with quasi-crystals can be found in the stabilization mechanisms we have identified here for β-boron; however, in the present case it is the conversion of bonding types (from two to three-centers) that leads to the Fermi level adjustment. An interesting question is why other 3rd group atoms do not form

icosahedron-based elemental solids, similar to boron. In this respect, we note that recently Haussermann *et al*. performed DFT enthalpy curve calculations on the 3rd group elements, and their results suggest that, under negative pressures, both gallium and aluminum exhibit icocahedron-based structures[38].

In conclusion, we have used a coupled CEMC/*ab-initio* technique to perform the first global configuration search on β-boron that includes all of the experimentally known POS. The resulting DFT total energies (including ZPE) of a series of stable hR1280 systems were found to be lower than that of the allotrope α-boron. The presence of defects, or POS, helps reduce the electron deficiency of the perfect lattice and gives rise to three-center bonds characteristic of boron compounds, and to localized gap states. We find that the ground state of boron can be best described as a degenerate disordered semiconductor with self-doping sites, and this makes it the only known element of the periodic table with such characteristics.

This work performed under the auspices of the U.S. Department of Energy by Lawrence Livermore National Laboratory under Contract DE-AC52-07NA27344.

Figure captions:

Fig.1: The building blocks of β-rhombohedral boron: a) icosahedral B_{12} units (green balls) are located at the corners and the middle edges of the rhombohedral unit-cell. Two B_{28} units and an interstitial atom (gold balls) are located in the middle of the unit-cell. In b) through g) the locations of the partially occupied sites (POS) are represented by red and blue balls, with the same naming scheme used in Ref. [3]. In b) the B13 sites form trimmers in the B_{28} units (red balls), and in c) the B16 sites are located at the center of the hexagonal rings connecting the B_{12} units (red balls). In d) the B17 and in e) the B18 sites (blue balls) next to and surrounding the B13 sites are shown. Finally, in f) the B19 and in g) the B20 sites (blue balls) located at the middle of the hexagonal rings connecting B_{12} and B_{28} units are shown.

Fig.2: The relative *ab-initio* DFT total energies, including zero-point energy contributions, of α-rhombohedral boron (black triangle), perfect β-rhombohedral boron (red triangle, 105 atoms in the rhombohedral unit-cell), β-rhombohedral boron with only B13 and B16 POS from Ref. [9] (green triangle). The blue circles and the yellow squares are the *ab-initio* DFT total energies of hR1280 systems obtained in steps (iv) and (v) of the CEMC/*ab-initio* procedure (see text). Each symbol corresponds to the total energy of a single hR1280 structure (not an averaged value).

Fig.3: Isosurfaces of the square of maximally localized Wannier functions (MLWFs)[24,39] where the color represents the occupation (η), blue: $1 \geq \eta \geq 0.95$, and red: $\eta < 0.95$ (see the Supplemental Material 5 for additional details). The isosurface value is set at half of the maximum value of the square of the MLWF. Structure a) corresponds to the perfect hR105, where the electron deficient bonds are present near the hexagonal rings connecting the B_{12} units. Note that the center of the hexagonal ring coincides with the B16 POS. b) and d) demonstrate the effect of occupying a B19 POS. The red ball in b) is the location of a B13 vacancy and the red ball in d) is the B19 atom (occupied). Comparison of b) and d) clearly demonstrates the elimination of electron deficient bonds [the red isosurfaces in b) and the absence of the red isosurfaces in c)] and 2-center to 3-center bonding conversion [the blue triangular isosurface around the red ball in d)]. c) and e) illustrate the termination of dangling (deficient) bonds created by two B13 vacancies. The two red balls in c) correspond to the location of the B13s, and the two red balls in e) are the B17-B18 pair. Note that no red isosurfaces are present in e).

Fig. 4: Participation functions of eigenstates from one of the 1280 atom supercells of β-boron and the hR105 perfect β-boron. The participation function, defined as $\xi_i = \int_V dr \frac{1}{|\Psi_i(r)|^4}$, where $\Psi_i(r)$ is the i^{th} eigenstates of the system and V is the volume of supercell, represents the localization length scale of the eigenstate.

[1] R. E. Hughes, C. H. L. Kennard, K. G. Sullenger, H. A. Weakliem, D. E. Sands, J. L. Hoard, *J. Am. Chem. Soc*. **85**, 361 (1963).

[2] J. L. Hoard, D. B. Sullenger, C. H. L. Kennard, R. E. Hughes, *J. Solid State Chem*. **1**, 268 (1970).

[3] G. A. Slack, C. I. Hejna, M. F. Garbauskas, J. S. Kasper, *J. Solid State Chem*. **76**, 52-63 (1988).

[4] There are experimental reports of the transition temperature from α-rhombohedral to β-rhombohedral boron. The transition is believed to be irreversible (no transition from β- to α-boron has ever been observed), and "*a large increase in the time required for the transformation with decreasing temperature was observed, indicating a large activation energy*."[5], clearly indicating that the α to β "transition temperature" discussed in the literature is not the thermodynamic limit, in conflict with the interpretation of Ref. [9]

[5] J.-O. Carlsson, *J. of the Less-Common Metals* **70**, 77 (1980).

[6] The DFT total energies of other polymorphs of boron have been intensively studied, and none of them was found to be as stable as α-rhombohedral boron at zero pressure. See, for example, Ref. [7] and Ref. [38]

[7] C. Mailhiot, J. B. Grant, and A. K. McMahan, *Phys. Rev. B* **42**, 9033 (1990).

[8] D. L. V. K. Prasad, M. M. Balakrishnarajan, E. D. Jemmis, *Phys. Rev. B* **72**, 195102 (2005).

[9] A. Masago, K. Shirai, H. Katayama-Yoshida, *Phys. Rev. B* **73**, 104102 (2006).

[10] M. J. van Setten, M. A. Uijttewaal, G. A. de Wijs, R. A. de Groot, *J. Am. Chem. Soc.* **129**, 2458 (2007).

[11] S. Shang, Y. Wang, R. Arroyave, Z.-K. Liu, *Phys, Rev. B* **75**, 092101 (2007).

[12] Although the three center bond of boron might seem unusual, the bonding scheme was first explained in terms of a simple linear combination of atomic orbitals description more than 40 years ago. For isolated trimmer configurations, see Ref. [13]. For more general cases, including extended systems, see Ref. [27].

[13] P. J. Durrant and B. Durrant, *Introduction to Advanced Inorganic Chemistry, John Wiley & Sons INC, New York,*134 (1962).

[14] The B16 POS was first reported in Ref. [2], and the rest of the POS, B17-B20 were first reported in Ref. [3].

[15] In Ref. [8] and Ref. [9], the atomic density was fixed at 105 atoms per rhombohedral cell, while in Ref. [11], atomic densities corresponding to 104, 105, 106, and 111 atoms per cell were examined. However, only the occupation of B13 and B16 POS in their simplest possible configurations were considered. For example, with 106 atoms per cell they considered only one POS configuration where all B13 sites and one B16 site were occupied.

[16] Setten *et al*.[10] derived their stable structures with 106 atoms in the rhombohedral cell by proposing candidate structures based on previous experimental work as well as intuition; they did not systematically explore the POS configuration space within the hexagonal cell (or a larger supercell).

[17] The number of possible configurations is calculated as follows: The 1280 atom supercell contains 12 rhombohedral cells. In the rhombohedral cell the position of 99 atoms correspond to fully occupied sites. This number is obtained by adding the total number of sites for B1-B12, B14, and B15. The number of each site can be found in Ref [3]. Note that the numbers reported in the literature are for the hexagonal cell, so one should divide by three to obtain the numbers used here. In the 1280 atom supercell 99×12=1188 atoms have coordinates corresponding to fully occupied sites. Therefore, 1280-1188=92 atoms have coordinates corresponding to POS. The total number of possible POS in the 1280 atom supercell is (6+6+6+6+6+12)×12=504. Finally, the 92 POS atoms can be distributed over the 504 sites, which corresponds to $\begin{bmatrix}504\\92\end{bmatrix}$ possible configurations.

[18] Z. W. Lu, S.-H.Wei, A. Zunger, *Phys. Rev. B* **44**, 2 (1991).

[19] G. D. Garbulsky, G. Ceder, *Phys. Rev. B* **51**, 67 (1995).

[20] C. Wolverton and A. Zunger, *Phys. Rev. Lett.* **81**, 606 (1998).

[21] The deviation of the cell-parameters from rhombohedral symmetry was negligibly small in all of our simulations.

[22] During the second iteration, several different constraints (described in the Supplemental Material 3) were used to examine potential biases that could come from the limitations of the cluster expansion Hamiltonian.

[23] The ZPE of both α- and β-boron were calculated from the full phonon dispersion using the linear response theory implemented in the PWSCF code. Additional details can be found in the Supplemental Material 4. For β-boron, the perfect hR105 system was used, and its ZPE was 8.2 meV/atom lower than that of α-boron. The impact of POS occupation was estimated by the sums of Γ-point phonon frequencies of the two most stable hR107 systems. This yielded a difference of 3 meV/atom, with respect to the energy of the perfect hR105. Therefore, we expect that the use of the hR105 structure to compute the ZPE (instead of hR107) has no impact on our conclusions regarding the relative stability of β- and α-boron. Note: The lower symmetry of hR107 would prohibitively increase the computational cost of the full phonon calculations.

[24] I. Souza, N. Marzari, D. Vanderbilt, *Phys. Rev. B* **65**, 035109 (2002).

[25] E. D. Jemmis, M. M. Balakrishnarajan, P. D. Pancharatna, *J. Am. Chem. Soc.* **123**, 4324 (2001).

[26] The perfect hR105 has five hole states per rhombohedral cell in the valence band. If one assumes that the number of valence bands does not change upon the introduction of POS atoms, the hole states would be perfectly filled at an atomic density of 106 2/3 per rhombohedral cell (the experimental value). Our finding is that the stable hR1280 systems nearly satisfy this condition, except for the small deviation originating from the presence of B17-B18 pairs. See the Supplemental Material 5 and 7 for additional details.

[27] H. Tang and S. Ismail-Beigi, *Phys. Rev. Lett*. **99**, 115501 (2007).

[28] O. A. Golikova, M. M. Kazanin, S. Samatov, T. Khomidov, *Sov. Phys. Semicond*. **16**, 479 (1982).

[29] H. Werheit, M. Laux, U. Kohlamann, *Phys. Stat. Sol*. (b) **176**, 415 (1993).

[30] R. Kubo, *J. Phys. Soc. Jpn.* **12**, 570 (1957).

[31] D. A. Greenwood, *Proc. Phys. Soc. (London)* **71**, 585 (1958).

[32] T. Takeuchi, S. Murasaki, A. Matsumuro, U. Mizutani, *J. Non-Cryst. Solids* **156-158**, 914 (1993).

[33] W. Ohashi, F. Spaepen, *Nature* **330**, 555 (1987).

[34] P. Bancel, P. A. Heiney, Phys. Rev. B 33, 7917 (1986).

[35] J. Friedel, *Helv, Phys. Acta*. **61**, 538 (1988).

[36] A. P. Smith, N. W. Ashcroft, *Phys. Rev. Lett.* **59**, 1365 (1987).

[37] T. Fujiwara, T. Yokokawa, *Phys. Rev. Lett*. **66**, 333 (1991).

[38] U. Haussermann, S. I. Simak, R. Ahuja, B. Johansson, *Phys. Rev. Lett.* **90**, 065701 (2003).

[39] A. A. Mostofi, J. R. Yates, Y.-S. Lee, I. Souza, D. Vanderbilt, N. Marzari, *Comput. Phys. Commun*., submitted (2007). See also, www.wannier.org.

Ogitsu_figure 1

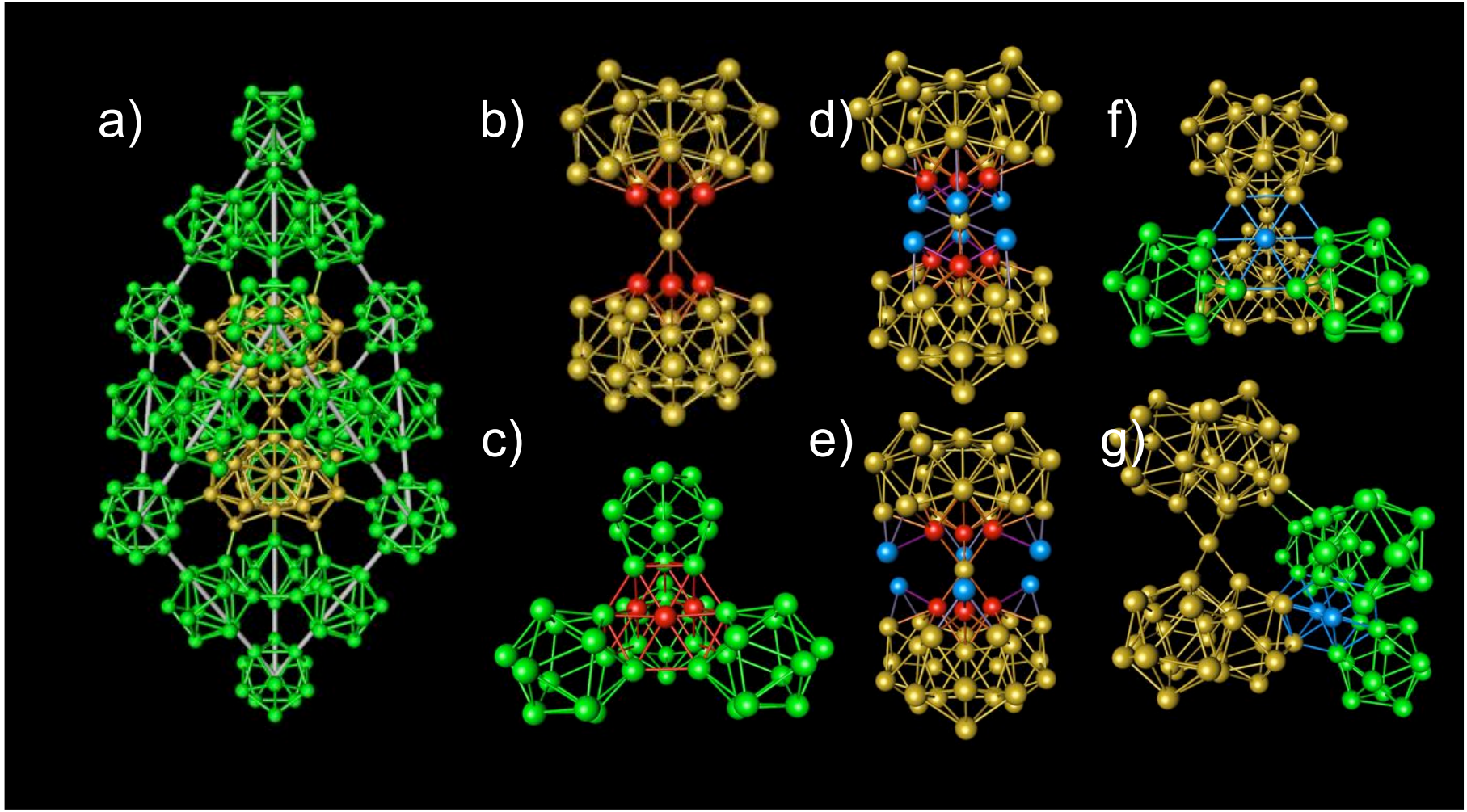

Ogitsu_figure2

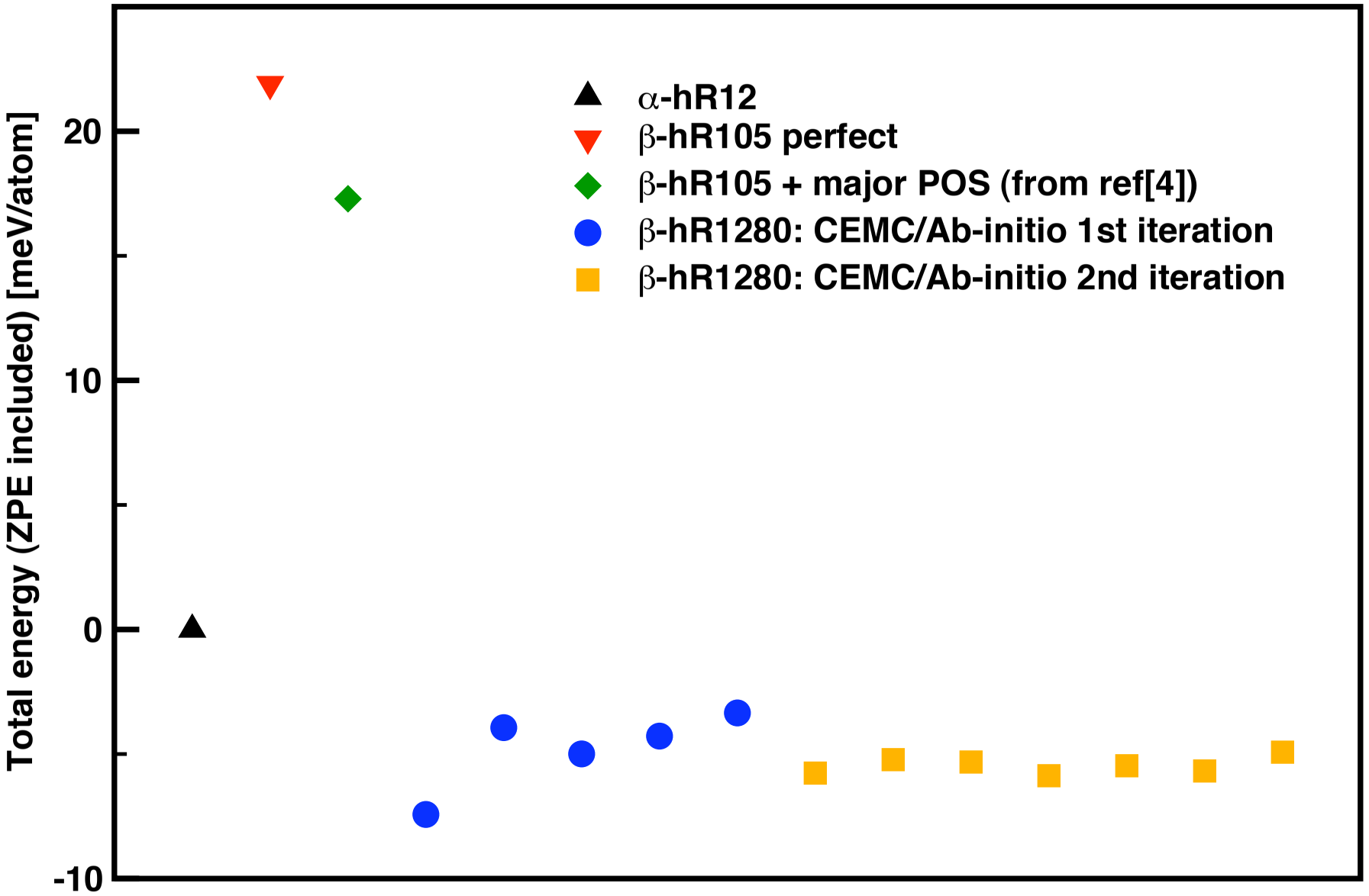

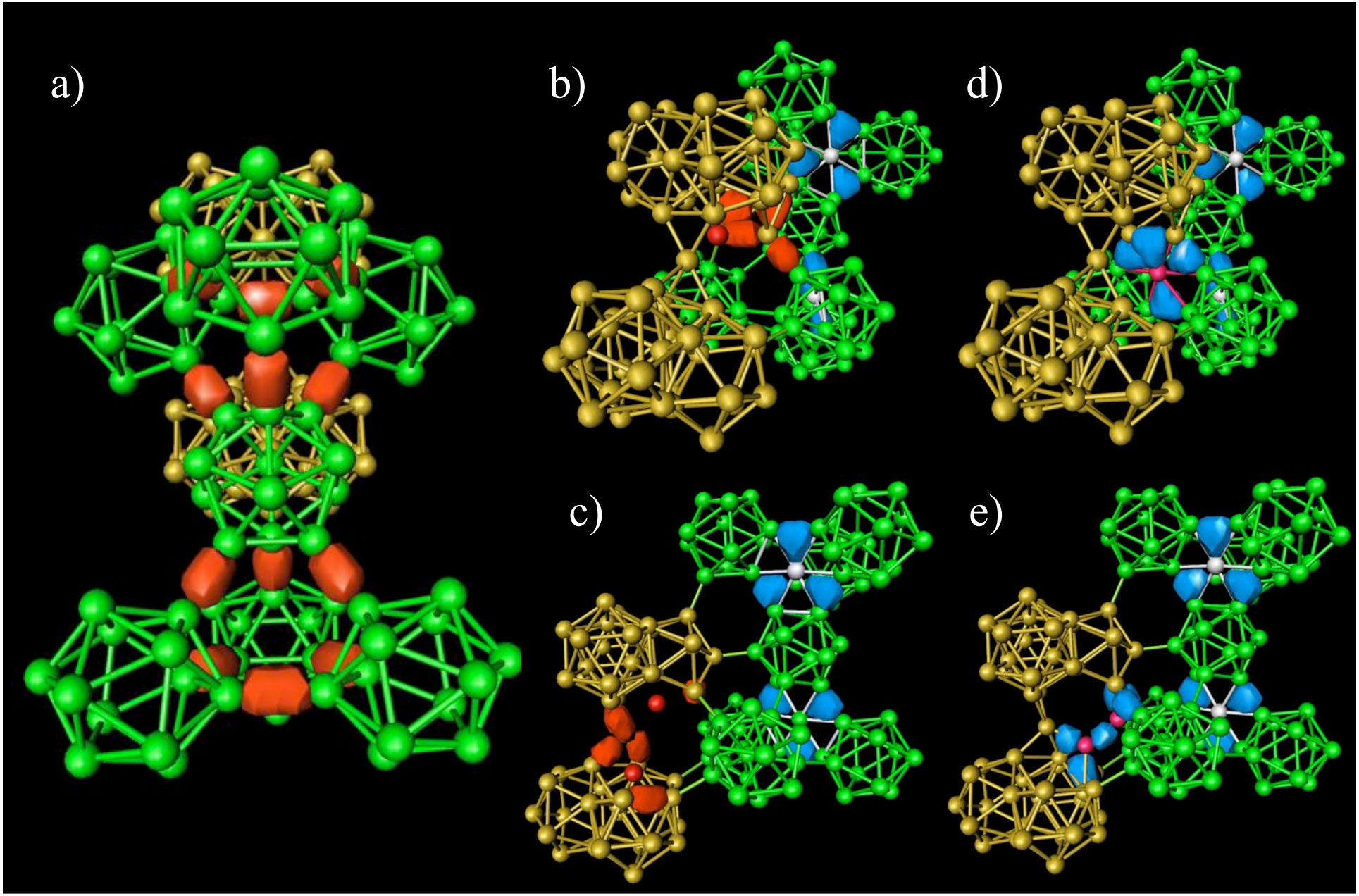

Ogitsu_figure 3

Ogitsu_figure4

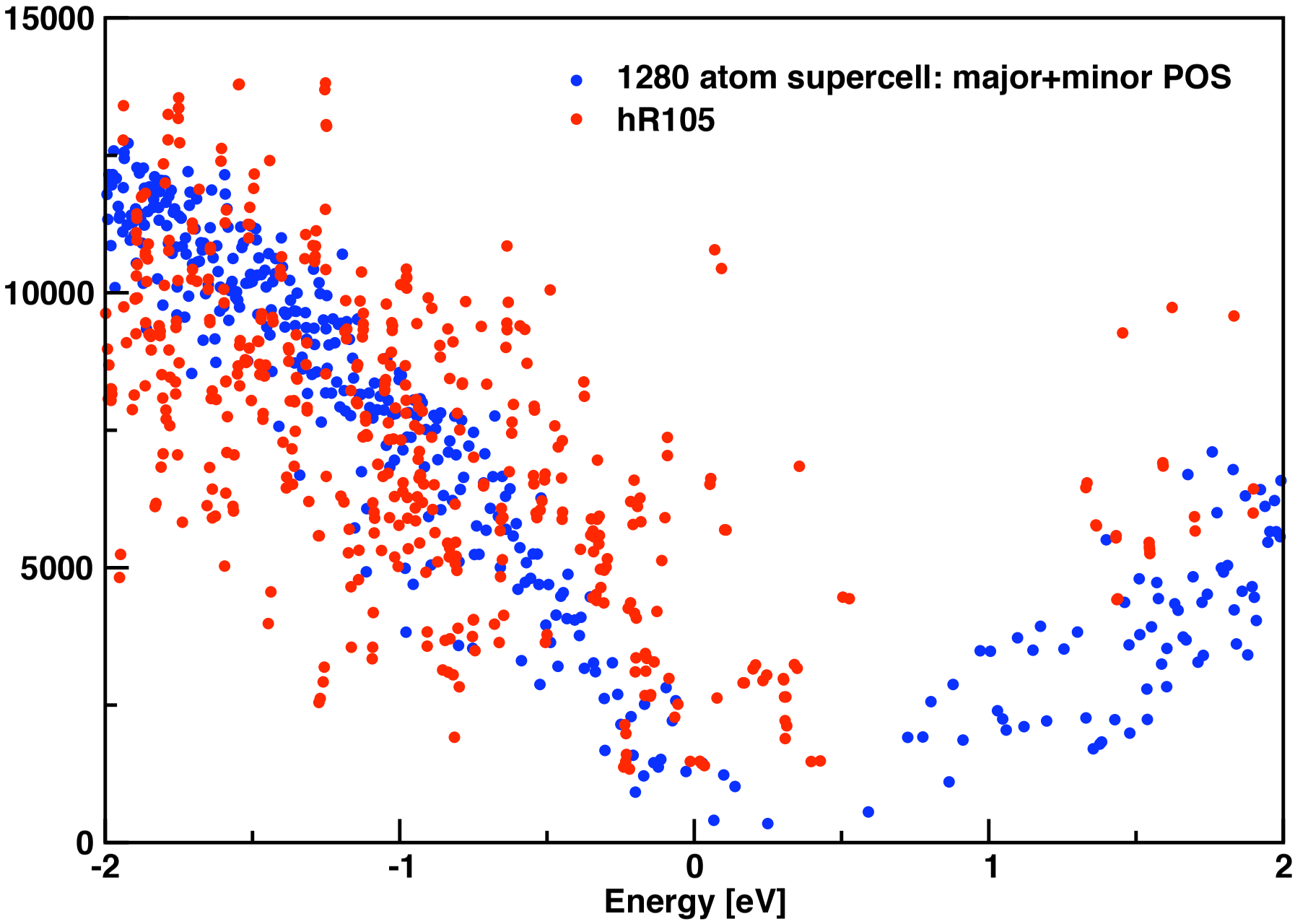

Supplemental Material 1: General Methods

For all of our total energy calculations, except for the Cluster Expansion Monte Carlo (Ref. [19-21] in the manuscript) for the configuration space search, we have used density functional theory (DFT)[1,2] within the local density approximation (LDA)[3,4] unless otherwise noted. Our total energy comparisons involved both the comparison between different unit-cell sizes (α-rhombohedral boron and β-rhombohedral boron) and the comparison between equivalent unit-cells (different POS occupations in β-rhombohedral boron), which require different settings of calculations (described later). To perform the individual calculations in the most efficient manner, we have used three different *ab-initio* DFT codes, GP[5] and Qbox[6] codes written by François Gygi (co-author) and the PWSCF code distributed at www.quantum-espresso.org. For all of our calculations, we have used the planewave expansion scheme with norm-conserving Troullier-Martins optimized pseudopotentials[7] for ions. The consistency on the basis set (cutoff energy), the pseudopotential, the exchange-correlation potential, was always kept for the individual comparisons. The numerical accuracies of the three codes were tested with identical calculation conditions, and it was confirmed that agreement over 8 digits was possible (i.e., the discrepancy was on the order of 10^{-3} meV/atom or less).

Our goal is to compare the total energies between α-rhombohedral boron (12 atom cell) and β-rhombohedral boron with the optimized POS occupation (1280 atom cells). Maintaining the same level of accuracy for these two systems is challenging for the following two reasons. One is the finite size effect on the electrons, and the other is the physical approximation, namely the LDA. First, we discuss the possible error coming from LDA. Then, we discuss how we deal with the finite size effects for these two very different systems. The details concerning the choice of the calculation parameters as well as an accuracy assessment will follow.

It is often believed that the reason why LDA (GGA) provides very accurate energy difference between two systems is that, in many cases, the error in the absolute energy of each system cancels each other when the difference is taken. Of course, this will not be the case if the LDA (GGA) error in the each system varies significantly. For example, the LDA error on the dissociation energy of molecule is known to be relatively large. One of the common explanations of this problem is the difference in the localization length, that is, an atom has a more localized electronic eigenstates than those of molecule, therefore, the binding energy of a molecule is usually overestimated within LDA (meaning that the relative total energy of an atom to that of a molecule is too high compared to that of the exact value). Considering this general trend, it is likely that the LDA error does not have an impact on our conclusions. In particular, the perfect β-boron has quite similar bonding

---

[1] P. Hohenberg and W. Kohn, *Phys. Rev*. **136**, B864 (1964).
[2] W. Kohn and L. J. Sham, *Phys. Rev*. **140**, A1133 (1965).
[3] D. M. Ceperley and B. J. Alder, *Phys. Rev. Lett*. **45**, 566 (1980).
[4] J. P. Perdew and A. Zunger, *Phys. Rev. B* **23**, 5048 (1981).
[5] F. Gygi, *GP 1.24.0: A General Ab Initio Molecular Dynamics Program* (Lawrence Livermore National Laboratory, Livermore, CA, 2003).
[6] F. Gygi, *Qbox, a large-scale parallel implementation of First-Principles Molecular Dynamics*, http://eslab.ucdavis.edu/.
[7] N. Troullier and J. L. Martins, *Phys. Rev. B* **43**, 1993 (1991).

properties with α-boron, and the LDA errors in the two structures should be very similar. When the POS atoms are introduced, as it is seen in the Fig 4 of the manuscript, the overall average localization of occupied states does not change, although the variation at a fixed energy is reduced (localization is enhanced only near the gap). Therefore, we expect that the impact of LDA error on our results is minor, and our conclusion should not be significantly affected. In addition, we have made a number of comparisons between LDA and GGA (described in the next section), which provides further support that our conclusions are not biased by the use of LDA.

Next, due to the large difference in the size of unit-cells between α-boron and β-boron, particularly when the POS atoms are included, very careful attention has to be paid on the error coming from the finite size effect on the electrons, *i.e., k*-point sampling. For this reason, a comparison was made in two steps. The first step involves comparing α-boron and perfect β-rhombohedral boron (no POS) with the irreducible cell (105 atoms in the rhombohedral cell), where absolute convergence on the *k*-points sampling can be achieved. The second step is to compare β-rhombohedral boron with and without POS occupancy. In the second step, we used a very large supercell (12 times that of the rhombohedral cell), and the total energy comparison was made between the same choice of the supercell and the same *k*-point sampling (Γ-point), which ensured that the finite size errors are equivalent between the two structures. The calculation parameters used to compute the energies reported in Figure 2 of the manuscript were selected so that the total energies of perfect β-boron computed with *k*-point sampling in irreducible cell and with Γ-point sampling in a supercell are equivalent. All of the other energies, α-boron and β-boron with POS, were computed within this framework. The details of the calculation parameters and the assessment of accuracy in these steps are further explained in the Supplemental Material 2.

Note: In the first step, a higher planewave cutoff energy (40 Ry) was used than in the second step (30 Ry) since the first step is potentially more sensitive to the cutoff energy. The reason is as follows. The planewave basis set for a given system is defined by both the cutoff energy and the unit-cell. Therefore, the basis set defined by the different sizes of unit-cells (but the same cutoff energy) can have different accuracies due to the discontinuous cutoff on the Fourier coefficients. This is essentially the same problem that is encountered with variable cell simulations, where the total energy changes discontinuously when the cell size changes due to an abrupt change in the number of Fourier coefficients. This error should be negligibly small as long as the cutoff energy is large enough so that the Fourier coefficients of the planewaves beyond the cutoff energy are essentially zero. In practice, when very large supercells are used, absolute convergence with respect to the cutoff energy is not feasible. On the other hand, when the total energy comparisons are made on exactly the same unit-cell and the same cutoff energy, this type of error does not take place since the basis sets of those systems are equivalent. Because of above reasons, we have used a larger cutoff energy for the first step than the second step (40 Ry for the first step, while 30 Ry for the second step). As it is described in the Supplemental Material 2, the validity of these choices is carefully verified with a few selected cases.

Pseudopotentials and LDA vs GGA:
For all of the DFT total energy calculations, the planewave/pseudopotential approach has been taken, where a norm-conserving Troullier-Martins optimized pseudopotential was used[8]. For all of the structural optimizations, the *s*-nonlocal and *p*-local configuration type pseudopotential was used for boron. The core cutoff radius, r_c=1.670 au, was used for all the angular momentum states. For a few randomly selected supercell systems (1260 atoms per cell and 1280 atoms per cell), the energy difference calculated with this pseudopotential was compared with those calculated with a more accurate pseudopotential, *i.e.*, *s*- and *p*-nonlocal, *d*-local. The change due to the difference in the pseudopotentials was negligibly small. The Purdue–Zunger LDA[4] was used for all the DFT results presented in our manuscript as well as the Supplemental Material. For the same set of supercell systems mentioned above, a comparison on the DFT total energy differences between LDA and the PBE GGA[9,10] was made. in all cases, the differences in energies were less than 3 meV/atom. Note: Setten *et al*. (ref [10] in the manuscript) used the PW91 GGA[11,12], where their total energy of the perfect β-boron relative to α-boron is +26 meV/atom (4 meV/atom smaller than our estimate with LDA). Therefore, our estimate on the relative total energy of hR1280 systems to that of α-boron should be higher than the GGA value. Assuming the general trend that GGA total energies are more accurate than LDA energies, it is reasonable to expect that the exact relative total energy of β-boron to that of α-boron is likely to be lower than our estimate based on LDA.

Accuracy of our calculations:
Here we list the lattice parameters and the bulk modulus calculated in this work together with experimental values and a few other DFT results. Our results are in excellent agreement with the available experimental data and the previous calculations. This indicates that LDA accurately describes the physical properties of the bulk phase of boron.

---

[8] The fhi98PP program package was used to generate all the pseudopotentials used in this work. See http://www.fhi-berlin.mpg.de/th/fhi98md/fhi98PP/ for the detail of this program package.
[9] J. P. Perdew, K. Burke, M. Ernzerhof, *Phys. Rev. Lett*. **77**, 3865 (1996).
[10] The pseudopotential is also regenerated with PBEGGA.
[11] J. P. Pewdew, K. Burke, Y. Wang, *Phys. Rev. B* **54**, 16533 (1996).
[12] J. P. Perdew, *in Electronic Structure of Solids `91*, edited by P. Ziesche and H. Eschrig (Akademie Verlag, Berlin, 1991), p.11.

	a [A] (rh)	α	a [A] (hex)	c [A]	B_0 [GPa]	B_0'
Exp1[13]	10.145±0.015	65°17′±8′	10.944	23.811		
Exp2[14]	10.17±0.05	65°12′±20′	10.959	23.887		
Exp3[15]	10.139	65°20′	10.945	23.787		
Exp4-1[16]			10.932(1)	23.818(3)		
Exp4-2			10.930(1)	23.815(3)		
Exp4-3			10.930(1)	23.815(3)		
Exp4-4			10.925(1)	23.810(3)		
Exp4-5			10.932(2)	23.819(5)		
Exp5[17]			10.934(11)	23.79(3)	185(7)	
Exp6[18]	N/A	N/A	N/A	N/A	210(6)	2.23
Exp7[19]	N/A	N/A	N/A	N/A	205(16)	4.3(1.6)
DFT1[20]	10.02	65.09°	10.78	23.56		
DFT2[21]	10.14	N/A				
DFT3[22]	9.996	65.22°	10.774	23.474	203.5	4.5
This work 1	9.957	65.38°	10.755	23.350		
This work 2			10.789	23.530		
This work 3					208.79	3.19
This work 4					208.33	3.22

Table S1-1: The theoretical and experimental lattice constants, bulk modulus and its pressure derivative of β-boron.

The optimized structure of Setten *et al.* can be found with the following link: http://pubs.acs.org/subscribe/journals/jacsat/suppinfo/ja0631246/ja0631246si20060504_105848.cif. Note: Their cell parameters deviate from rhombohedral symmetry, therefore, to avoid confusion, we did not include this in the table. The cell parameters in Exp1-3 were given for the rhombohedral cell, while the rest are given for the hexagonal cell. The experimental data, from Exp 4-1 to Exp4-5, correspond to the five different samples listed in the Table VII of Ref. [16], MG77, MG57, MG79, MG179, and Eagle Picher, respectively. Note: The differences between the MG samples are the cooling rate when

[13] R. E. Hughes, C. H. L. Kennard, D. B. Sullenger, H. A. Weakliem, D. E. Sands, and J. L. Hoard, *J. Amer. Chem. Soc*. **85**, 361 (1963).
[14] Von D. Geist, R. Kloss and H. Follner, *Acta Cryst*. **B26,** 1800 (1970).
[15] Bengt Callmer, *Aca Cryst* **B33**, 1951 (1970).
[16] G. A. Slack, C. I. Hejna, M. F. Garbuskas, and J. S. Kasper, *J. Solid State Chem*. **76**, 52 (1988).
[17] R. J. Nelmes, J. S. Loveday, and D. R. Allan, *Phys. Rev. B* **47**, 7668 (1993).
[18] D. N. Sanz, P. Loubeyre, and M. Mezouar, *Phys. Rev. Lett*. **89**, 245501 (2002).
[19] Y. Ma, C. T. Prewitt, G. Zou, H.-k. Mao, and R. J. Hemley, *Phys. Rev. B* **67**, 174116 (2003).
[20] J. Zhao and J. P. Lu, *Phys. Rev. B* **66**, 092101 (2002).
[21] D. L. K. Prasad, M. M. Balakrishnarajan, and Eluvathingal D. Jemmis, *Phys. Rev. B* **72**, 195102 (2005)
[22] A. Masago, K. Shirai, and H. Katayama-Yoshida, *Phys. Rev. B* **73**, 104102 (2006)

they were solidified. In Exp5, a linear fit was used to obtain the bulk modulus (B_0), therefore, B_0' is not given. This is most likely due to the narrow pressure range that they measured in their experiments (compared to Exp6 and Exp7). In the Exp6, the Vinet fit was used to calculate B_0 and B_0', while in Exp7, Birch-Murnaghan equation of state was used. We have tested the difference coming from the different equation of state models. The B_0, and B_0' in 'This work 3' is calculated by the Vinet fit, while the ones in 'This work 4' is calculated by the Virch-Murnaghan fit. This indicates that the difference coming from the fitting functions should be negligible as long as the equations of state curve itself is well defined. The equation of state itself for those calculations are the same one obtained with a 1280 atom supercell (320 atoms per hexagonal cell). For this, we have calculated the P-V relation at the four different pressures, 0Gpa, 25GPa, 50GPa, and 75GPa. The parameters in 'This work 1' are calculated with the perfect hR105 (no POS), which is 105 atoms in the rhombohedral cell. The parameters in 'This work 2' are calculated with one of the 1280 atom supercell (320 atoms per hexagonal cell) structures. The POS configuration dependency on the lattice parameters was negligibly small.

For the convenience of the readers, we summarize the various calculation details used in the theoretical results listed in the previous table.

	Pseudopot	Cutoff	*k*-points	LDA/GGA	# of atoms/Unit-cell
DFT1	Ultra-soft[23]	240eV	3^3 (rh-cell)	GGA[24]	105/rhombohedral
DFT2	Ultra-soft[23]	N/A	N/A	GGA[9]	105/rhombohedral
DFT3	TM[7]	40Ry	Γ-point	LDA[4]	105/rhombohedral
This work 1	TM[7]	40Ry[25]	3^3	LDA[4]	105/rhombohedral
This work 2-4	TM[7]	30Ry[25]	Γ-point	LDA[4]	1280/supercell (320/hex-cell)

Table S1-2: The calculation scheme and the parameters for the DFT results listed in Table S1-1.

[23] D. Vanderbilt, *Phys. Rev. B* **41**, 7892 (1990).
[24] Y. Wang and J. P. Perdew, *Phys. Rev. B* **43**, 8911 (1991)
[25] Checked up to 60Ry. See the supplemental material 2.
[27] The electronic density of states (EDOS) of this system is shown in the supplemental material 7.

Supplemental material 2: Comparison of total energies of β- and α-boron allotropes: Assessment of convergence of *ab-initio* calculations.

Two key parameters controlling the convergence of plane-wave-pseudopotential electronic structure calculations are the size of the plane wave basis set (expressed in terms of kinetic energy cutoff—E_{cut}) and the number of points used to sample the first Brillouin zone (or number of *k*-points--N_k). When the total energies of different crystal structures of a given system are compared, it is particularly important to check the convergence with respect to N_k, especially so when the unit cell sizes of the two structures are significantly different. The unit-cell of β-boron is roughly an order of magnitude larger than that of α-boron. Therefore, we have conducted a careful assessment of the convergence of our calculations with respect to *k*-point sampling.

We first examined the convergence of the total energy difference ($\delta E_{\alpha\beta}$) between α- and β-boron with respect to E_{cut}. For each allotrope, both the atomic positions and the cell parameters were optimized until the maximum force became less than 0.001 Ry/au, and the total stress was less than 0.1 GPa. These calculations showed that $\delta E_{\alpha\beta}$ with E_{cut} = 40 Ry differs by less than 1meV/atom from that computed with E_{cut} = 60 Ry. Therefore, we chose E_{cut} = 40 Ry for our *k*-point convergence study. For systems with different cell sizes, a comparable number of sampling points in the Brillouin zone is given by the number of atoms in the unit-cell multiplied by N_k. In Fig. S2.1 we show the total energy as a function of this parameter for both α- and β-boron.

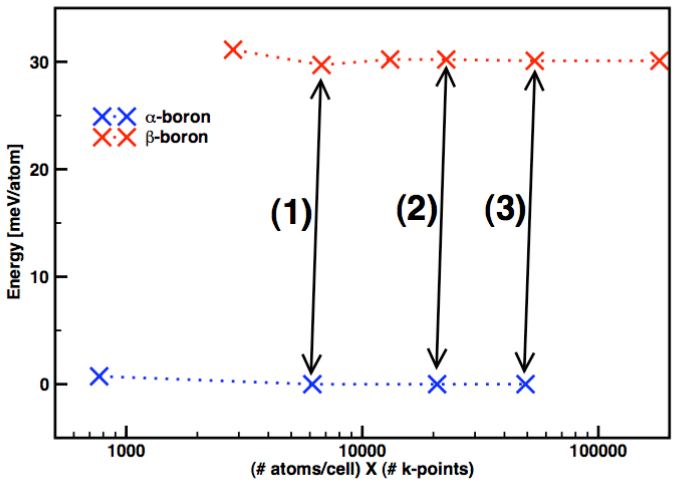

Figure S2.1: The total energy as a function of the "system size" (the number of *k*-points multiplied by the number of atoms). The 'system size' unit is introduced to approximately measure the longest Bloch wave vector for a given unit-cell and the *k*-points grid. The longest Bloch wavelength for a given unit-cell and a number of *k*-points

can be calculated as follows. Suppose we have a cubic cell with its dimension $L \times L \times L$, and the *k*-point sampling is N^3. The smallest k-vector will be, for ex., $2\pi/(NL)(1,0,0)$, therefore its wavelength is NL. If you take cubic of the wavelength, it becomes $(NL)^3$, this is the volume of unit-cell multiplied by the number of *k*-points. Now, we have two different systems, which have different unit-cell volumes but its atomic densities are more or less the same. One may replace the number of atoms in the cell with the volume of the cell to approximate this 'system size parameter' if the atomic densities are similar.

When determining the energy difference between α- and β-boron, one should, in principle, use the perfectly converged limit of the *k*-points grid size. Indeed, the densest grid we have used has a very good convergence, about 1 meV/atom change with an incremental change in the grid size (see Figure S2.1). However, the energy scale of interest is comparable to 1 meV/atom, so one should select the closest "system size" between the α-boron and β-boron calculations to minimize the impact of system size effects. It is natural to expect that the size effect on electrons could be defined as a function of the longest Bloch wave vector defined by the unit-cell and the *k*-point grid, which is roughly proportional to (the length)^3 of the longest Bloch wave vector *k* (thus the measure of size effect on electrons). In the present study, systematic comparisons were made for three cases: (1) N_α=6144 and N_β=6720, (2) N_α=20736 and N_β=22680, (3) N_α=49152 and N_β=53760, for which we found the following energy difference: (1) $\delta E_{\beta-\alpha}$=29.66 meV/atom, (2) $\delta E_{\beta-\alpha}$=30.22 meV/atom, and (3) $\delta E_{\beta-\alpha}$=30.09 meV/atom. We used result (3) as our best computed value of the energy difference between α- and β-boron. This value is slightly smaller than the one reported by Masago *et al*. (Ref. [9] of the manuscript). We believe that the more stringent convergence criteria used in our calculation accounts for this small discrepancy. We also note that the total energy computed for β-boron exhibits an unexpectedly large sensitivity to size effects, which we attribute to the presence of a Fermi surface in the perfect β-boron lattice (α-boron is a conventional semiconductor). This sensitivity to *k*-point sampling may also contribute to the discrepancy between our and Masago *et al*.'s results, as the Γ-point only was used in Ref. [9] of the manuscript.

When determining the energy difference between the perfect β-rhombohedral boron and our 1280 boron atoms supercell results (referred as hR1280 in the manuscript), we used a different approach. The perfect hR105 was modeled with a 1260 atoms supercell, and the total energy was calculated with exactly the same parameters as the hR1280 systems, that is, E_{cut}=30Ry with Γ-point sampling and both the atomic positions and the cell parameters optimized until the maximum force becomes less than 0.0005 au and the stress on the simulation box becomes less than 0.01 GPa. This energy is taken as the origin for the energies of hR1280 systems relative to the perfect hR105.

Supplemental material 3: Details of the POS optimization procedure using the lattice model Monte Carlo simulated annealing and *ab-initio* total energy calculations

To achieve a high efficiency in the global search of the POS configurations, we model the POS in β-boron with a lattice model Hamiltonian, particularly the Cluster Expansion method. Therefore, we will call this optimization procedure the CEMC/*ab-initio* optimization method hereafter. In the Cluster Expansion Hamiltonian, the interaction is described by the site occupation energy (site local) and the pair interaction. The higher order terms (eg. three body interaction) are omitted for simplicity.

Choice of atomic configurations for β-boron 106 and 107 atom cells:
As mentioned in the manuscript, even if we use rhombohedral cells with 107 atom/unit cell, the number of possible configuration attainable in a β-lattice with partially occupied sites (POS) is huge, i.e. approximately 150 million (symmetry equivalent structures are redundantly counted here). Therefore, we reduce the number of POS configuration by limiting them to physically meaningful configurations within a rhombohedral unit-cell. The following criteria were used: 1) the standard deviation of the atomic coordination number from 6 was required to be less than 1.4; and 2) the occupation of site B13 (N_{B13}) was restricted to be $2/3 \leq N_{B13} \leq 1$, and that of site B16 to be $0 \leq N_{B16} \leq 1/3$. The constraint on atomic coordination numbers was meant to minimize the number of dangling bonds and the number of over coordinated atoms in the system. 2) was motivated by the results of *ab-initio* structural optimization on samples with 1280 atoms/unit cell where the POS occupation was configured in a random manner[27]. These calculations showed that having more than two vacancies per triangle at B13 sites distorted the B_{28} unit to the extent that cannot be compatible with experimental observations. We also found that more than two boron atoms in a single B13 triangle make the B16 site unstable. Therefore, those POS configurations were excluded from our fitting.

Fitting of the lattice model Hamiltonian:
After selecting a unique set of atomic configurations with the procedure described above, we obtained 2591 independent configurations that include 106 and 107 atoms in a rhombohedral unit-cell. *Ab initio* total energy calculations were performed for all of these structures and the resulting energies were used to fit the parameters in the Cluster Expansion model Hamiltonian. The type of Hamiltonian is a generalized Ising lattice model Hamiltonian, where the occupation of each site, either vacancy or occupied, was mapped onto a spin model (vacancy = -1 i.e. Spin down and occupied = +1 i.e. Spin up). The local site occupation and the pair correlation coefficients for each POS were fitted using the mean square fitting method. The cutoff radius (r_{cut}) for the longest pair correlation included was chosen to be r_{cut} = 3.5A, which covers the second nearest neighbors (see the pair correlation function of β-boron in Fig. S3.1). A weighting factor with an exponential form, $\exp[-k(E_i-E_{lowest})]$, with E_i equal to the energy of a particular structure was used in the mean square fitting procedure in order to bias the fit towards low energy structures. Although the effect of this factor on the absolute total energy values was small, we found that it was necessary to include it in order to achieve a correct energy sequence for the lowest energy structures. Additional details of the procedure followed here can be found in Ref. [19-21] in the manuscript.

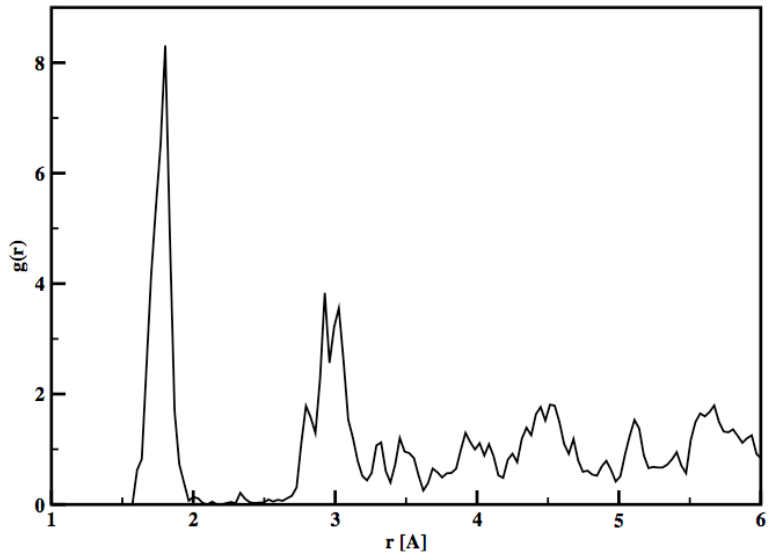

Fig. S3.1: The pair correlation function of β-boron. The cutoff radius, 3.5A, is slightly larger than the 2nd nearest neighbor distance. The 1280 atoms supercell was used for this calculation. The atomic positions are relaxed using *ab-initio* structural optimization. In β-boron, bond lengths vary between different units, e.g., intra-B_{12}/B_{28}, the inter B_{12}-B_{12} linkages, and the inter B_{12}-B_{28} linkages. Furthermore, the presence of POS atoms induces a slight broadening of the main peaks and gives rise to small peaks in between the main ones.

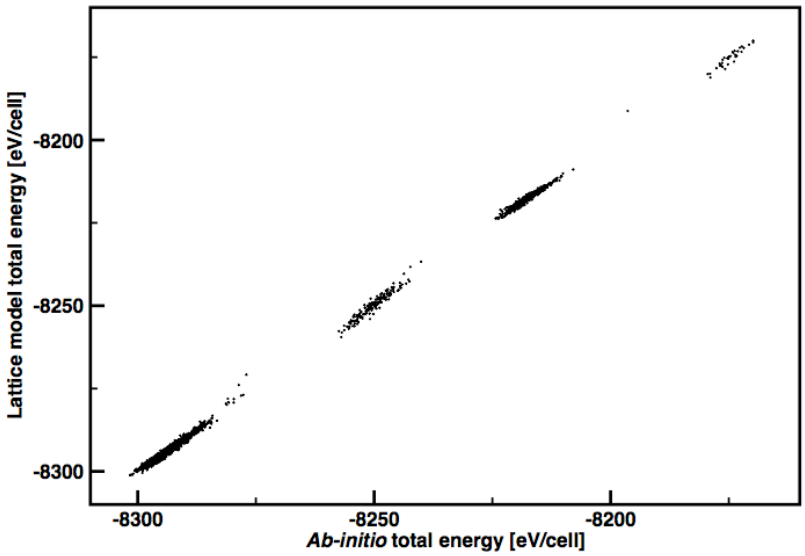

Figure S3.2: Comparison of total energies computed from *ab-initio* calculations and those obtained using a generalized Ising lattice model Hamiltonian.

CEMC optimization using the simulated annealing technique:
Using the coefficients determined by fitting *ab-initio* total energies for 106 and 107 atom unit cells to their respective sets of characteristic site and pair correlations, we constructed a spin Hamiltonian that was used for rapid energy calculations of supercells containing 1280 atoms (2x2x3 repetition of a primitive unit-cell). A simulated annealing procedure using the Metropolis algorithm (and with various cooling rates and number of Monte Carlo steps) was then performed to search for ground state configurations of POS atoms. The simulated annealing consistently output ground state structures with an identical set of site and pair correlations, for a given Hamiltonian. However, the specific atomic structures varied between annealing cycles, as the lattice Hamiltonian did not account for longer-range pair correlations, or higher order multi-body correlations, that could break up the lattice model ground state degeneracy. Therefore, we observe the small fluctuations in the final *ab-initio* total energies (see Fig 2 of the manuscript).

Refitting of the Hamiltonian for an additional iteration of CEMC/*ab-initio* simulations
Ab-initio total energy calculations with and without full structural optimizations were performed for several 1280 atom supercell boron configurations generated by the CEMC

optimization described above. Using these energies in combination with the previously calculated 106 and 107 atom cell energies, two separate Hamiltonian re-parameterizations were carried out: one for energy calculations allowing only electronic relaxation, and the other using the energies of full structural optimizations. The two different sets were designed to test the sensitivity of pair interactions to small structural variations. Using the relaxed total energies usually gave better final results (i.e. predicted structures with lower *ab-initio* total energies), although there were a few notable exceptions.

Let us briefly justify the coupled *ab-initio*/CEMC procedure adopted in our study. The lattice model is an approximation to the *ab-initio* total energy, and it is introduced to accelerate the search in the global configuration space. This model was used as a means of systematically generating candidate supercell structures that then warranted further analysis with more exact but far more time-consuming *ab-initio* calculations. Many CEMC optimizations were performed that produced different annealed structures. The variation in output structure was achieved by: 1) fitting the spin Hamiltonian to energy calculations allowing only for electronic relaxation, and fitting the spin Hamiltonian to calculations including also structural optimizations; 2) by varying cooling rates and number of steps in annealing cycles, for a given Hamiltonian; 3) by adding additional constraints on site occupancy so as to allow structures which were not ground states of the lattice model, but were still relatively low in energy, to be considered. This set of candidates included structures constrained to have the experimental occupation rates, N_{B17}:N_{B18}:N_{B19}:N_{B20} (see Table S2.1). We have chosen roughly 50 lowest energy (of the lattice model Hamiltonian) configurations, several each from each constraint, and further optimized the atomic positions as well as the cell parameter using *ab-initio* DFT method as described below.

The final step (*ab-initio* structural optimizations):
To screen all the candidate structures generated by the CEMC optimizations, *ab-initio* structural optimizations were performed starting from the CEMC optimized structures with a loose convergence criteria, e.g. the maximum force acting on an atom, $F_{max,}$ was chosen to be less than 0.01 au. Several lowest energy configurations from these partially optimized structures were then selected, and further relaxed with $F_{max} < 0.0005$ au and with the stress on the simulation box less than 0.01 GPa. Note that the change in the POS configuration leads to negligibly small changes in the optimized cell parameters.

The resulting *ab-initio* total energies including the ZPE are reported in Fig. 2 of the manuscript. The occupation rates of these seven structures are shown in Table S2.1. Interestingly, none of our low energy structures possessed exactly the same occupation as that extracted from experiment. Instead the relative occupation between B13-B20 could fluctuate significantly, with an energy variation of less than a few meV/atom, indicating the nearly degenerate character of β-boron. Our results suggest that the occupation rates extracted from experiment may correspond to high temperature equilibrium values. Most likely, in the real β-boron samples the POS configuration does not reach its ground state due to kinetic limitations. In fact, the diffusion onset found for POS atoms in our *ab-initio* molecular dynamics simulations suggests that barrier heights for diffusion are of the order of 1000 K.

Name	*B13*	*B16*	*B17*	*B18*	*B19*	*B20*	*Total energy [meV/atom]*
CEMC_1_A	79.167	30.556	4.167	4.167	8.333	0.694	0.774456925
CEMC_1_B	69.444	30.556	13.889	13.889	0	0	6.699310489
CEMC_1_C	66.667	27.778	16.667	16.667	0	0	6.046662464
CEMC_1_D	80.556	29.167	2.778	2.778	4.167	4.167	3.610393292
CEMC_1_E	70.833	30.556	12.5	12.5	0	0.694	3.321272343
CEMC_2_A	70.833	31.944	12.5	12.5	0	0	3.274502778
CEMC_2_B	79.167	33.333	4.167	4.167	6.944	0	2.993885386
CEMC_2_C	76.389	33.333	6.944	6.944	4.167	0	2.876961473
CEMC_2_D	70.833	30.556	12.5	12.5	0	0.694	2.730275109
CEMC_2_E	72.222	33.333	11.111	11.111	0	0	2.517686176
CEMC_2_F	73.611	31.944	9.722	9.722	2.778	0	2.432650603
CEMC_2_G	73.611	33.333	9.722	9.722	1.389	0	2.328482026
EXP A	77.7(14)	25.8(13)	3.2(8)	5.8(15)	7.2(14)	0	N/A
EXP B	74.5(6)	27.2(7)	8.5(9)	6.6(6)	6.8(5)	3.2(4)	N/A
EXP C	73.0(5)	28.4(5)	9.7(7)	7.4(6)	7.0(5)	2.5(25)	N/A

Table S2.1: The occupation rates in the final structures from the 1st iteration (CEMC_1_[A-E]) and 2nd iteration (CEMC_2_[A-H]) of CEMC/*ab-initio* simulations. The zero of the total energy was set at the energy of the α-boron structure, and the quantum Zero Point motion Energy (ZPE_β-ZPE_α=-8.2meV/atom) was not included here. Large fluctuations were observed in the occupation rates; N_{B13} = [66.667, 80.556], N_{B16} = [27.778, 33.333], N_{B17} = [2.778, 16.667], N_{B18} = [2.778, 16.667], N_{B19} = [0.0, 8.333], N_{B20} = [0.0, 4.167].

The experimental values (EXP A, EXP B, and EXP C) are taken from Ref. [3] in the manuscript. The names of the samples in their paper are MG57 (A), EP (B), and MG179 (C), respectively. A faster cooling rate was used for MG57 than for MG197. Also, the site, B17, is different from the ones for EP and MG179. It is referred as B17d site in their paper. Probably, the faster cooling rate prevented to reach its (high temperature) equilibrium position.

Supplemental material 4: Phonon Density of States and Quantum Zero Point Motion Energy (QZPE) of α and β allotropes.

To evaluate the ZPE and the Helmholtz free energy of elemental boron, we performed full phonon dispersion curve calculations using the PWSCF program version 2.1.5, distributed at www.pwscf.org, which is a part of the quantum-espresso package, distributed at www.quantum-espresso.org. In the following, *k* is a wave vector specifying a Bloch state of electron, while *q* is the wave vector of a phonon mode.

Computational strategy:
We first performed *ab-initio* structural optimizations for both α- and β-boron structures. Structural optimizations were considered as converged when the maximum force F_{max} was smaller than 0.0008 Ry/au, and the total stress was less than 0.001 GPa. For each *q*-point, a set of wavefunctions were calculated and, using linear response, phonon frequencies were obtained. A relatively coarse *q*-point grid was used in our calculations. Phonon frequencies on a denser grid were then obtained by means of a Fourier interpolation scheme in order to insure convergence of the ZPE and of the Helmholtz free energy with respect to the integration over the first BZ.

Choice of parameters:
In our phonon calculations we used E_{cut} = 40 Ry for both α- and β-boron. For the integration of Bloch electronic states in the 1st BZ, 12^3 *k*-points for α-born, and 3^3 *k*-points for β-boron, were used with a Monkhorst-Pack grid. The phonon calculations were performed on a coarse linear grid of points in the BZ (*q*-point), 4^3 *q*-points for α-boron, and 3^3 *q*-points for β-boron. By using Fourier interpolation, the phonon density of states was then calculated on 12^3 *q*-points grids for both α- and β-boron.

Results for ZPE and Helmhotz Free Energy:
The phonon density of states of α- and β-boron are shown in Fig. S4.1. The zero point motion energy, $\mathrm{ZPE} = \sum_s \int_{BZ} dq \frac{1}{2}\hbar\omega_{s,q}$, where $\omega_{s,q}$ is the phonon frequency of the s^{th} branch at the wave vector *q*, are ZPE_α = 133.8 meV/atom and ZPE_β = 125.6 meV/atom, for α- and β-boron, respectively. The difference $\delta_{ZPE} = \mathrm{ZPE}_\beta - \mathrm{ZPE}_\alpha$ = -8.2 meV/atom was added to the total energies of all β-boron structures in Fig. 2 of the manuscript. The vibrational contribution to the Helmholtz free energy difference between α-and β-boron is given in Fig. S4.2. It is seen that the vibrational free energy contribution stabilizes β- over α-boron at all temperatures, which is consistent with the fact that β- is softer than α-boron (i.e. its bulk modulus is smaller).

Instability of the perfect β-lattice:
For the perfect β-lattice, at *q*- (0,0,0), five eigenvalues of the dynamical matrix are imaginary values. We have simply replaced these values with zero, in order to calculate the ZPE and the Helmholtz free energy. In the following, we explain why this approximation is justified, and why it does not affect our conclusions on the stability of β-boron at T = 0 K.

By inspecting the corresponding eigenvectors, we can classify three of the five

eigenmodes with imaginary frequency as acoustic modes. The absolute values of these frequencies are very small, 6.3 cm^{-1}, 6.3 cm^{-1} , and 7.6 cm^{-1} (0.78 meV , 0.78 meV , and 0.94 meV). Given the numerical accuracy expected in our phonon calculations, it is a reasonable approximation to set these three frequencies to zero.

The remaining two degenerate modes, with $|\omega|$=209.6 cm^{-1}, turned out to be stretching modes involving atoms that participate in "electron deficient" bonds (see Fig. S4.3 (a) and (b)). Our analyses of bonding properties (see manuscript) show that such modes are likely present only in the perfect β-boron structure, since the nature of some electron deficient bonds is changed by the presence of POS. Therefore, neglecting these modes when computing the ZPE of the defective β-structure, appears to be justified. The upper bound of the error coming from neglecting these two modes can be estimated by considering the highest phonon frequency of β-boron: ω_{max} ~ 1300 cm^{-1}. The maximum error is $2*\omega_{max}$/(number of atoms = 105) ~ 3.0 meV/atom, which is smaller than the ~5-7 meV/atom energy difference between α- and β-boron (see Fig. 2 in the manuscript).

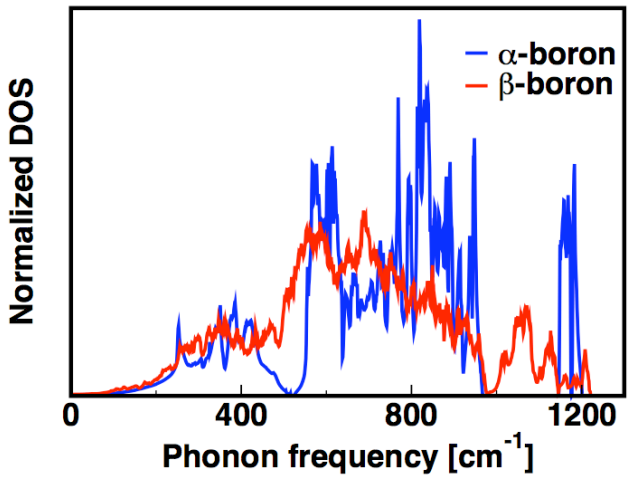

Figure S4.1: The phonon density of states of α- and β-boron, as obtained using *ab-initio* calculations.

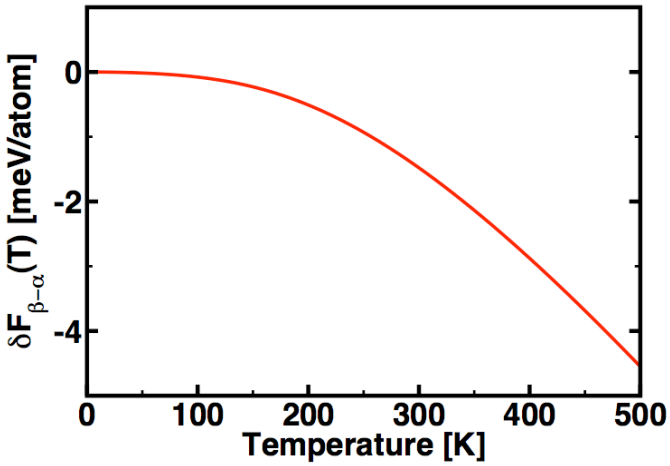

Figure S4.2: The vibrational contribution to the Helmholtz free energy difference between α- and β-boron.

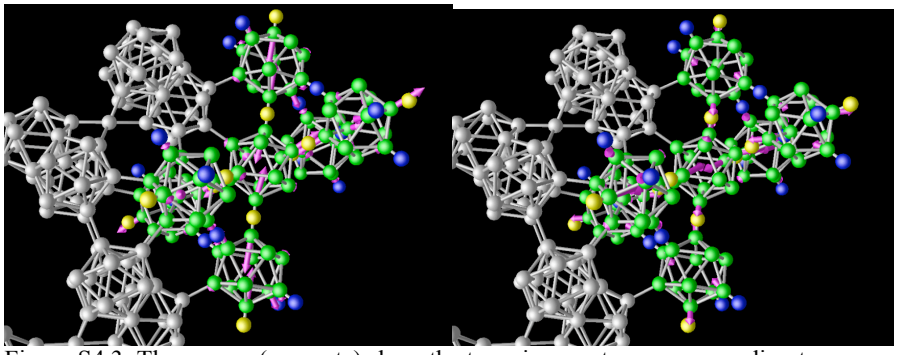

Figure S4.3: The arrows (magenta) show the two eigenvectors corresponding to imaginary eigenvalues of the dynamical matrix of the perfect β-boron structure. The green and the grey spheres represent boron atoms. B_{12} icosahedrons are green, and $2(B_{28})B$ units are grey. The yellow and blue spheres represent the position of the MLWF centers (see text). Orbitals with different occupation numbers (see text for definitions) are shown by different colors (either yellow—those with the lowest occupation, less than 0.9, or blue—those with occupation within [0.9,0.95]).

Supplemental material 5: Analysis of bonding properties: Maximally Localized Wannier Functions (MLWF)

In this work, we use Maximally Localized Wannier Functions (MLWFs) constructed from the eigenfunctions to identify the bonding types in β-boron. The MLWFs are known to provide a qualitative description of chemical bonding, for example, in an sp^3 bonded system such as diamond, the MLWFs represents each σ-bond well. However, it is also known that there are a few cases where the MLWFs do not reflect the bonding character well. For example, in a sp^2 bonding system such as graphite, the σ-bonds and the π-bonds are mixed, and the resulting MLWFs do not resemble either σ-bonds or π-bonds. Souza, Marzari and Vanderbilt have shown that by applying their disentangled MLWF method, one can generate MLWFs for an sp^2 system, where each MLWF keeps the character of either a σ or a π bond (see the Ref. [24] of the manuscript). To apply this disentanglement method, one has to first identify the character of each eigenfunctions. On the set of the bands having the same character, the MLWF transformation is applied to avoid mixing between different types of bonds.

In our MLWF analysis, we have identified the character of each eigenstate, and have examined several different disentanglement schemes (different ways to separate the bands). Our analysis indicates that the character of inter B_{12} and/or B_{28} bonds are always qualitatively well reproduced in the MLWFs independent of our disentanglement scheme[28]. The only exceptions are the lowest set of eigenstates separated by a gap, which have not been used in any of our analysis. These MLWFs have delocalized *s*-like character and are located inside the B_{12} and B_{28} clusters. All the rest of the eigenstates have hybridization between intra and inter units (B_{12} and B_{28}) bonds, however, they could be qualitatively sorted as follows. The next lowest set of eigenstates correspond to either intra-B_{12} or intra-($2B_{28}$)B bonds. They are not two-center bonds, however, not exactly three-center bonds either (described, for example, in Ref. [25] of the manuscript). Overlapping with these intra-cluster like eigenstates, there are two different types of eigenstates inter-connecting between the B_{12} and/or the B_{28} units. Among them, the three center-bonds are located lower in energy than two-center bonds. The two-center bonds connecting between B_{12}'s are the highest in energy.

Starting from electronic eigenstates obtained in our *ab-initio* calculations, we obtained the MLWFs for the β-boron structure with the Wannier90 program developed by A. Mostofi, J. Yates, I. Souza, N. Marzari, and D. Vanderbilt (Ref. [39] of the manuscript), and the GP code developed by F. Gygi [using the algorithm presented in: *Comp. Phys. Comm.* **155**, 1 (2003)]. The Wannier90 program is distributed at www.wannier.org.

The computational procedure and the choice of parameters:

We computed MLWFs for several β-boron primitive rhombohedral cells. For all of the calculations, 4^3 *k*-points on a uniform grid were used with E_{cut} = 20 Ry. The MLWFs for the perfect β-hR105 were also calculated with E_{cut}=40 Ry, and compared with those calculated with E_{cut} = 20 Ry. No essential difference was found between the results obtained with the two different E_{cut} values; therefore, all of the MLWF calculations were

[28] If the choice of bands is not appropriate, some or all MLWF will take either unphysically large spread or complex value with relatively large imaginary component (a well defined MLWF should take only real values).

carried out with E_{cut} = 20 Ry. We tested the sensitivity of our results against the choice of initial conditions for the iterative procedure used to obtain MLWFs, We used randomly distributed *s*-type orbitals, as well as other random configurations. No difference in the spread and location of the resulting MLWFs was observed for all the configurations considered here.

We used 160 single particle eigenstates, which is the number of valence states below the excitation gap, to build MLWFs for all β-configurations except for one. In the case where the β-lattice contained a B17-B18 bond, an additional state above the Fermi level was considered, as this system has 161 valence eigenstates. The detail is discussed later.

The definition of occupation of MLWF:

If ψ_{mk} denote single particle eigenstates for the electrons, MLWFs are defined as: $w_{nR}(r) = \frac{V}{(2\pi)^3}\int_{BZ}[\sum_m U^k_{mn}\psi_{mk}(r)]e^{-ik\cdot R}dk$, where the unitary matrix U is defined in such a way as to minimize the spread, $\Omega = \sum_n [< w_{n0}(r) \mid r^2 \mid w_{n0}(r) > - \mid< w_{n0}(r) \mid r \mid w_{n0}(r) >\mid^2]$. Using this unitary matrix, the occupation of a WF is defined as $\eta'_{n0} = \frac{V}{(2\pi)^3}\int_{BZ}\sum_m U^k_{mn}\eta_{mk}dk$, where η are occupation of single particle electronic orbitals. Using this definition, we successfully classified electron deficient bonds, in a way that is consistent with phenomenological descriptions of 2- and 3-center bonds.

The spread of MLWF versus the bonding type in the perfect β-boron:

We first describe MLWFs of the perfect β-boron. Interestingly, the histogram of spread distributions has two groups of peaks represented by two relatively sharp and large peaks, one at Ω~1.3 and the other at Ω~1.5 (see Fig. S5.1). The MLWFs with the small spread group correspond to conventional 2-center-2-electron bonds, and those are the ones linking B_{12}-B_{12} or B_{12}-B_{28} units. The number of those bonds is 42. At about Ω=1.38, the character of MLWFs changes clearly. They correspond to either the intra-B_{12} bonds or the intra-2(B_{28})B bonds. Intra B_{12} bonds can be quantitatively defined by the Boronoi method and one obtains 13 MLWFs per B_{12} unit. To count the MLWFs belonging to the ($2B_{28}$)B unit is more complicated due to its complex geometry. However, if one uses the fact that (total number of bonds) = (B_{12} internal bonds)+(interconnection between B_{12}s and B_{28})+(B_{12} internal bonds), it can be calculated simply, that is, to subtract the 2-center-2-electron bonds (interconnections) and the number of internal bonds of B_{12} from the total number of bonds. The total number of bonds is considered to be equal to the number of valence bands, 160. Therefore, the number of intra-2(B_{28})B bonds is calculated as follows: (the total number of bonds)-(the number of B_{12}-B_{12} linkage plus the number of B_{12}-B_{28} linkage)-(the total number of the intra-B_{12} bonds), 160-42-(13)*4=66. Note that the factor 4 for the number of intra-B_{12} bonds comes from the number of B_{12} units in the rhombohedral cell. The number of bonds obtained in this way matches exactly that obtained using semi-empirical rules (see Ref. [25] of the manuscript; therefore, MLWFs can be seen as an *ab-initio* foundation for semi-empirical counting rules used to rationalize the bonding property of boron.

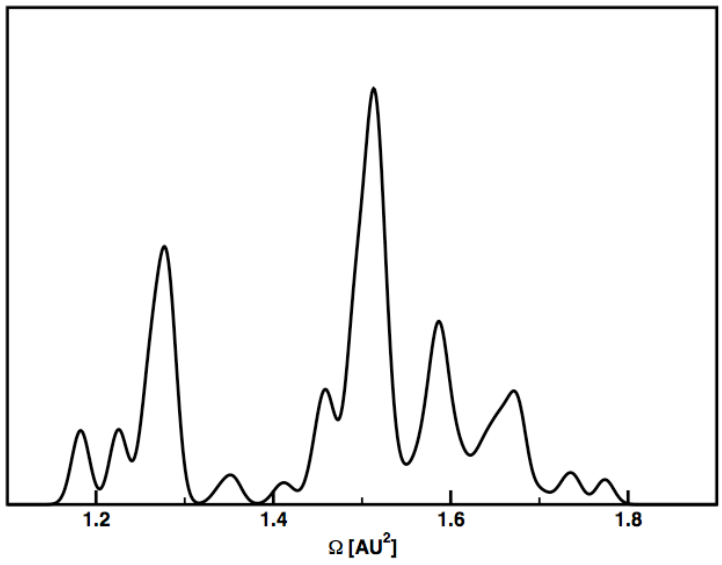

Fig. S5.1: The histogram of spread for the perfect β-hR105.

The electronic structures of low energy hR107 systems:
Here we show how the use of MLWFs to describe bonds leads to the identification of two stabilization mechanisms induced by the presence of POS in the structure of β-boron. The two mechanisms are: self-doping via the conversion of two-center to three-center bonds; and pairing of B17-B18 atoms, leading to the presence of gap levels.

We first note that the short-range correlations of POS seen in the stable structures, (a)-(d) in Fig. S5.2 for 107 cells, are the ones consistently seen in 1280 atom supercell calculations, as obtained from our CEMC/*ab-initio* optimization; this indicates that short-range correlations in the POS occupations are mostly responsible for the stabilization of the β-boron. The effect of long range correlations is most likely equal to or smaller than the energy fluctuations observed in the total energies of the stable 1280 atoms systems. Therefore, it is reasonable to assume that there is a strong analogy between the electronic structures of the hR107 and the 1280 atom cells.

We therefore considered the hR107 atom cells. Let us compare the location of the Fermi levels (E=0[eV], E_f). In the perfect hR105, the E_f lies in the valence band, and the number of hole states in the valence band (obtained by integrating the DOS between the E_f and the valence band top) is 2.5 (5 electrons). In (a), (b), and (d), the conduction band is partially occupied and the number of electrons in the conduction band is 1. Since 6 electrons were added (two boron atoms are added in this case), the number of valence band states did not change upon the addition of two POS atoms. In (c) (B17-B18 interstitial pairing), the same number of electrons (atoms) are added, E_f is in the valence band, and the number of hole states is one, meaning that one valence state was added by forming the B17-B18 pair.

At the correct chemical potential, i.e. 106 2/3 atoms per rhombohedral cell, (a), (b), and (d) become perfect semiconductors, while (c) (B17-B18 pair) has the E_f in the valence band. In fact, all of our stable CEMC/*ab-initio* optimized structures have E_f in the valence band as well as B17-B18 pairs. We have also performed constrained CEMC optimizations without a B17-B18 pair; these optimizations yielded structures with higher energy and hence were discarded.

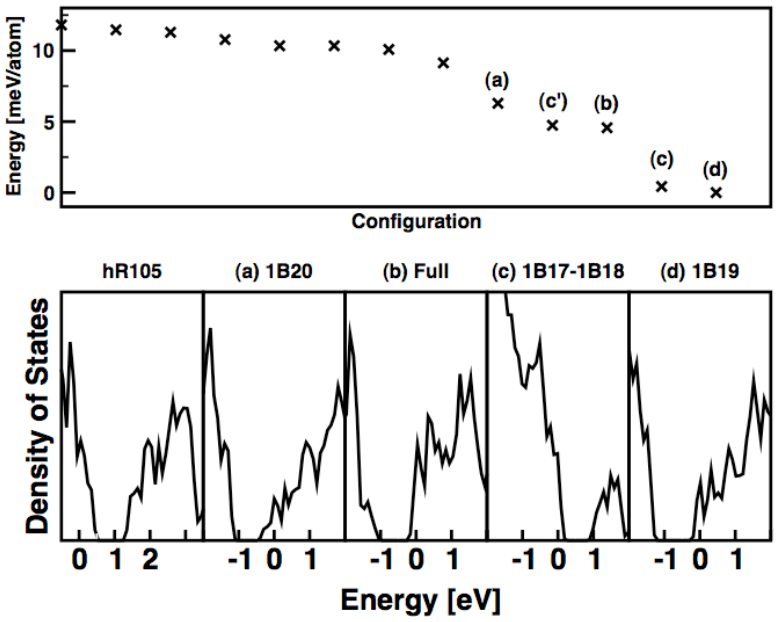

Fig. S5.2: Upper panel: Lowest 13 total energies of hR107 systems sorted by energy. Lower panel: The density of states of the five lowest systems separated by an energy gap. The left most one is the perfect β-rhombohedral boron. (a) 5B13-2B16-1B20. Five atoms in the B13 site, or one vacancy in the B13, as the number of B13 site is 6 per rhombohedral cell. Note: B13, B16-B19 has 6 sites each, while B20 has 12 sites. (b) 6B13-2B16. (c) 4B13-2B16-1B17-1B18 (B17-B18 pair). (d) 5B13-2B16-1B19. (c') 4B13-2B16-1B17-1B18 (B17-B18 pair), here, the relative position of B17-B18 pair to B16 is different from (c)).

The MLWFs analysis on the low energy hR107 systems:

We also calculated the MLWFs of the systems, (a), (b), (c), (d) of the Fig. S5.2 and the results are shown in Fig. S5.3. In configurations (a), (b), (d), it is seen that no additional MLWF are formed around the POS atoms; however, the location of MLWF centers are slightly pulled towards the POS atom. Those POS sites, B16, B19, and B20, are the center of hexagonal ring consisting of alternating three intra-cluster bonds and three inter-cluster bonds (see Fig 3 of the manuscript). Therefore, if three inter-cluster bonds (two-center) are converted to three-center bonds, the total number of bonding states remains unchanged. Due to the conversion of this bonding type from two-center to three-center, the POS atoms can shift up the E_f without changing the number of valence states. On the other hand, when a B17 site and a B18 site are occupied and forms the B17-B18 pair, another bonding state is introduced.

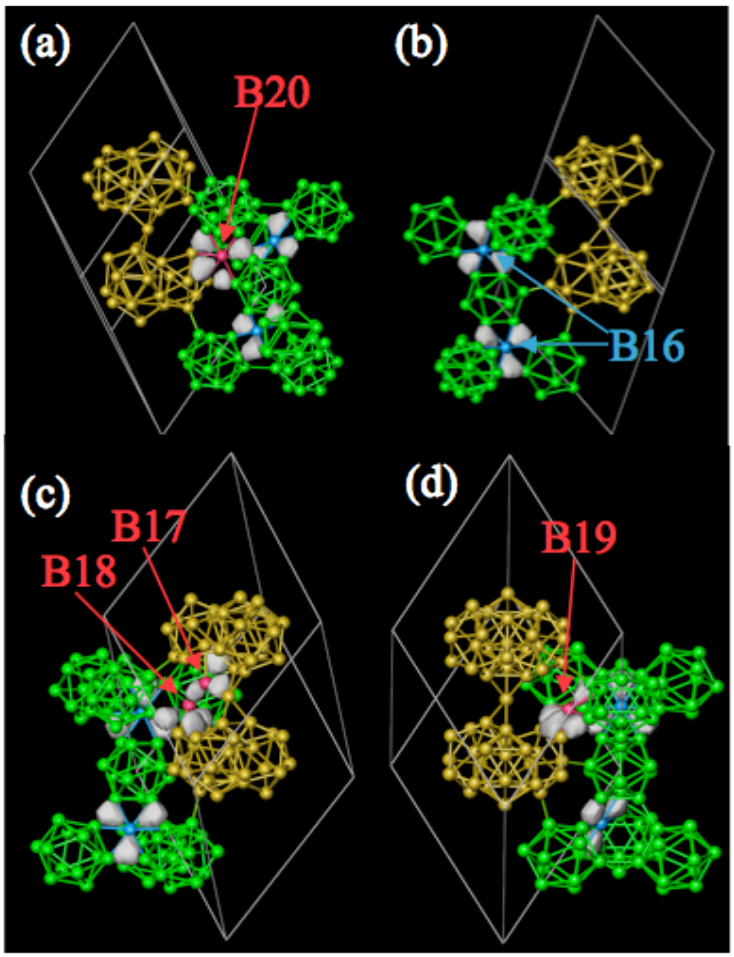

Fig. S5.3: The square modulus of the MLWFs for the systems, (a), (b), (c), (d) of Fig. S5.2. The iso-surface value is set at half of the maximum value of the square modulus of the Wannier function. The MLWFs plotted here are chosen as follows; the MLWF centers closer than 1.35A to the B16 atom(s) and the MLWF centers closer than 1.385A to the B17-B20 atoms. The conversions of bonding character from two-centre to three-centre are clearly seen near the B16, B19 and B20 atoms. Near the B19 atom and B20 atom [(a) and (d)] an additional MLWF is seen in each figure. They are terminating the dangling bond created by the B13 vacancy next to POS atoms (see Fig. 3 (b) in the manuscript as the comparison). In (c), a bond between the B17 atom and the B18 atom is formed and the other bonds nearby tend to hybridize with the dangling bonds near the B13 vacancies. The number of valance states is larger by one (see Fig. S5.2), compared to all the other systems in Fig. 3 in the manuscript, and those of Fig. S5.3.

Supplemental material 6: The entropic contribution to the Helmholtz free energy

The entropic contribution on the Helmholtz free energy as the function of temperature has been calculated from the *ab-initio* DFT total energies of the hR107 systems used to fit the lattice model Hamiltonian. The formula that we have used is as follows, $F(T) = -k_B T \ln\{\sum_j \exp(-\frac{E_j - E_0}{k_B T})\}$, here k_B is the Boltzmann constant, T is the temperature, E_j is the *j-th* hR107's DFT energy, E_0 is the lowest energy of all hR107 structures. The sum is taken for all the structures we have calculated. Note: this is an approximate way to estimate the actual free energy of macroscopic system. This value should correspond to an upper bound.

We emphasize that the free energy at ambient temperature in this plot reaches to -133 meV/atom.

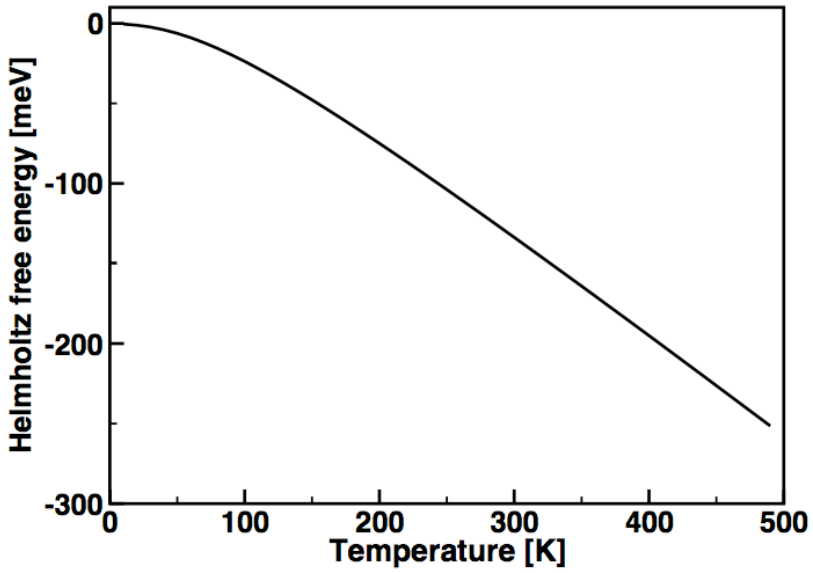

Fig S6.1: The entropic contribution on the Helmholtz free energy as a function of temperature.

Supplemental material 7: The electronic structures of hR1280 systems

The electronic density of states (EDOS) of some selected systems are shown to demonstrate the correlation between the stabilities and the band gap and/or the gap levels. Although the correlation here is not strictly true for all the cases, the overall trend is more or less described below.

The most stable hR1280 structure has a relatively clear gap (see Fig S7.1), however, there are a small amount of hole states in the valence band (0.5 states per rhombohedral cell), while most of the higher energy hR1280 structures either did not have a clear gap, or there were a significant amount of gap levels.

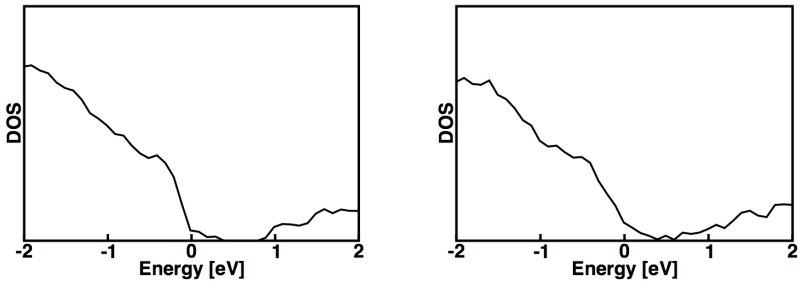

Fig S7.1: The EDOS of the most stable hR1280 structure (left). The electronic gap is about 0.8 eV, however, small amount of hole states are seen above the Fermi level (E=0eV). A clear gap is not seen in the right one, where the energy was roughly 6meV/atom higher due to the presence of unfavored B16-B19.

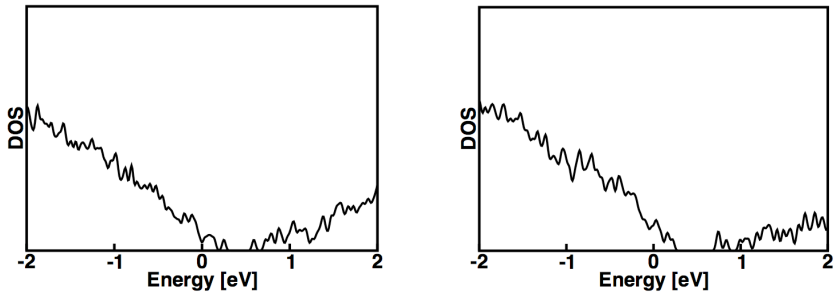

Fig S7.2: Left: The EDOS of the structure, which was about only 2 meV/atom higher than the most stable one. Right: The one, whose energy was 8 meV/atom higher than the most stable one. Clear gaps are observed in these EDOSs, although the number of hole states are slightly higher than the most stable one (see above).

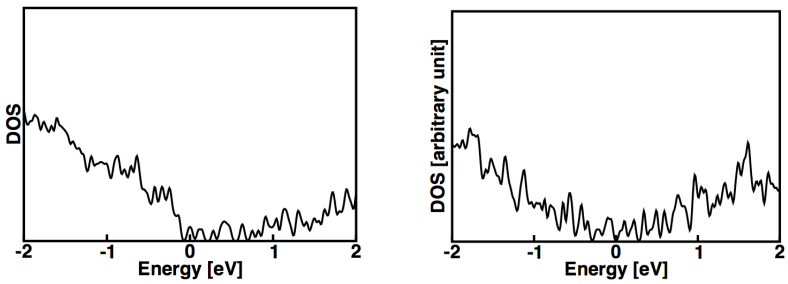

Fig S7.3: The EDOSs of two different higher energy configurations. Left: (16 meV/atom higher than the most stable one) B13-B20 are randomly occupied but the occupation rates are set as close as to the one in the Ref. [3] of the manuscript. Right: (12 meV/atom higher than the most stable one) B13 is fully occupied, and B17-B20 are not occupied. Number of B16 atoms are chose in such a way that the total number of atoms becomes 1280 (320 atoms per hexagonal cell). The B16's occupation configuration is configured with some consideration on its stability, that is, the unfavored configurations such as two B16 in a one triangle (see Fig 1 of text) were avoided, otherwise, the occupation configuration was chosen randomly.